Modelling the effects of nozzle geometry on the thermo-viscoplastic flow of solid deuterium during cryogenic extrusion

D. M. Takács*, B. Longauer*,**, M. Málics*,**, T. Szepesi*, E. Walcz*,** and T. Giegerich***
Corresponding author: takacs.donat@ek.hun-ren.hu
* HUN-REN Centre for Energy Research, Institute for Atomic Energy Research, Budapest, Hungary.
** Budapest University of Technology and Economics, Budapest, Hungary.
*** Karlsruhe Institute of Technology, Karlsruhe, Germany.

Abstract: For fuelling magnetic confinement nuclear fusion devices, the current leading approach is the injection of solid hydrogen (deuterium and tritium) pellets. The material for these pellets is produced via extrusion: this is possible since solid hydrogen isotopes at cryogenic temperatures behave as non-Newtonian thermo-viscoplastic fluids, with highly temperature-dependent material parameters. Here, we study the extrusion of solid deuterium.
The challenges of achieving an adequately high flow rate during the extrusion are mainly thermal, as the internal heat generation inside the material must be kept to such a level that the temperature of the material cannot reach its triple point temperature anywhere. Accurate prediction of the thermal behaviour of the material during extrusion necessitates the use of an accurate CFD model. In this work, we describe our approach for modelling the thermo-viscoplastic flow of solid deuterium inside an extruder. The model developed is used for exploring alternative geometries for the extrusion nozzle, with the goal of minimizing the maximum temperature developing inside the material.

Keywords: cryogenics, extrusion, deuterium, non-Newtonian fluids, thermo-viscoplasticity, fusion

1. Introduction

For magnetic confinement nuclear fusion devices, a continuous fuelling system is necessary for supplying hydrogen isotopes (deuterium and tritium) into the core of the plasma. The current leading, proven approach for this is the injection of solid hydrogen pellets: these are extruded and cut at cryogenic temperatures, before being launched into the plasma at high speeds [1, 2, 3].

Extrusion of solid hydrogen is possible above its yield stress, where it behaves as a non-Newtonian viscous fluid with strongly temperature-dependent material parameters [4]. Reliable numerical modelling of this plastic flow behaviour requires a coupled thermo-viscoplastic simulation with an appropriate material model. In some cases, constant material parameters are considered for easing the computational demand, but for more accurate results, the temperature-dependence of the thermal and mechanical material parameters cannot be neglected [5, 6, 7, 8].

A key goal of the numerical model is the accurate prediction of the heat generated due to viscous dissipation, since the temperature of the extruded material must remain below its triple point during extrusion to prevent melting: this usually limits the maximum achievable flow rate for a specific design. Furthermore, the dissipated heating power gives a lower bound on the cryogenic cooling power required for continuous operation, which can incur significant costs. Since the flow behaviour is highly nonlinear due to the non-Newtonian and temperature-dependent nature of the material, a CFD model is necessary for predicting its behaviour during extrusion.

This paper focuses on the effects of the nozzle geometry (i.e., the initial, contracting part of the die) on the resulting temperature distribution inside a cryogenic solid deuterium extruder. First, a FEM-based CFD model for the non-Newtonian flow of solid hydrogen inside the extruder is presented. Then, the effects of changing the nozzle geometry are considered. Including the reference geometry as a baseline, three different conical geometries, and two parabolic geometries are investigated.

2. Problem Statement

2.1 Reference setup

A prototype cryogenic hydrogen extruder of batch type (Fig. 1a) has been designed and built at the Fusion Plasma Physics Department of the HUN-REN Centre for Energy Research (EK-CER) [9]. It is capable of supplying a continuous solid deuterium rod of nominal diameter $\varnothing d_2 = 3.2$ mm (Fig. 1b) at a temperature of approximately 15 K, which is subsequently cut into separate pellets. The geometry and operation of this reference device is considered as the baseline for the calculations given in the following. Fig. 2 illustrates the geometry of the inside of the extruder, i.e., the axisymmetric flow domain for the deuterium ice.

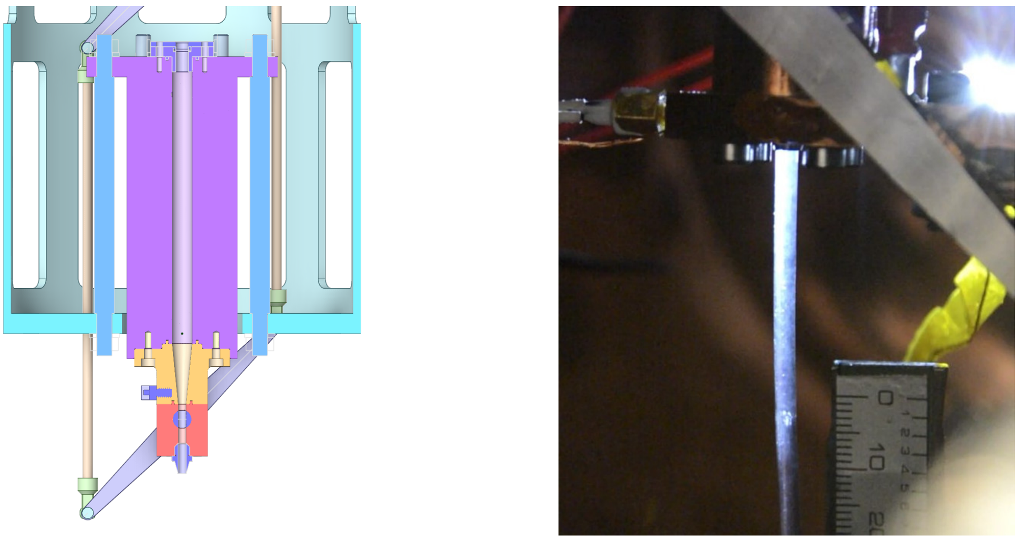

(a) (b)

Figure 1: Left: cross-sectional view of the extruder. Right: extruded solid deuterium rod. During extrusion, deuterium ice formed in the main copper cylinder (purple) is pushed by a piston moving inside the extruder (not shown), through a converging nozzle (orange) ending in a narrower tube of nominal diameter (red), which supplies the ice to the next device.

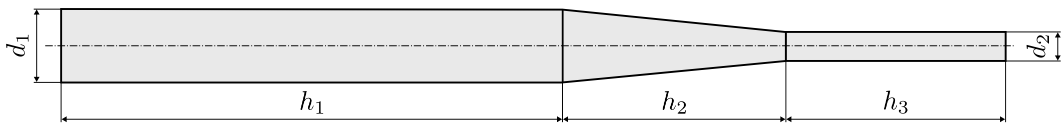

Figure 2: Sketch of the flow domain geometry inside the extruder. For the reference extruder, the lengths are $h_1 = 100$ mm, $h_2 = 24$ mm, $h_3 = 27.6$ mm, and the diameters are $d_1 = 8$ mm, $d_2 = 3.2$ mm

2.2 Basic material parameters

The thermal and mechanical material parameters of solid hydrogen isotopes exhibit considerable temperature-dependence. Experimental data is available in the relevant literature for basic material parameters such as density, specific heat and thermal conductivity, among others [10, 11].

It should be highlighted that even for pure deuterium isotope material, the ratio of the ortho- and para-deuterium spin isomers in a sample can influence the material parameters significantly: e.g., the peak thermal conductivity of pure ortho-deuterium is around one order of magnitude higher than that of normal deuterium. In the present case, we assume a normal (2:1 ortho-para) composition, as the deuterium gas being frozen is initially at room temperature and thus in approximately a normal state, and the freezing is considered fast enough such that the relaxation of the spin states to the cryogenic-temperature equilibrium can be neglected.

2.3 Constitutive model

While, for protium, two different constitutive models are commonly used for describing its viscous flow [12, 4], for deuterium, the most widely used correlation is the empirical model due to Leachman [4]. This model assumes that solid deuterium behaves as a non-Newtonian Herschel–Bulkley fluid with temperature-dependent parameters, i.e., the constitutive relationship for the viscosity is

$$\begin{cases} \dot{\gamma} = 0, & \text{if } \tau \leq \tau_0, \\ \tau = \tau_0(T) + \mu(T)\dot{\gamma}^n, & \text{if } \tau > \tau_0, \end{cases} \tag{1}$$

where τ is the shear stress, $\dot{\gamma}$ is the shear rate,

$$\tau_0(T) = a_1 \left(\frac{\nu_0 + a_5 T_\mathrm{m}^{a_6}}{\nu_0 + a_5 T^{a_6}} \right)^{a_2} \tag{2}$$

is the temperature-dependent yield stress,

$$\mu(T) = a_3 \left(\frac{\nu_0 + a_5 T_\mathrm{m}^{a_6}}{\nu_0 + a_5 T^{a_6}} \right)^{a_4} \tag{3}$$

is the temperature-dependent consistency index, and $n = 1/2$ is the flow index. The parameters $T_\mathrm{m}, \nu_0, a_1, a_2, a_3, a_4, a_5$ and a_6 of the expressions (2)–(3) are given[1] in [4]. Fig. 3 illustrates the constitutive relationship for various temperatures.

A consequence of the Herschel–Bulkley-type non-Newtonian fluid flow described above is the characteristic flow velocity profile with plug flow in the center [13, 14]: this is taken into account during the meshing.

2.4 Thermal considerations

The main difficulty of extruding solid hydrogen isotopes is managing the temperature distribution and channelling away excess heat. Crucially, the temperature of the material being extruded must not exceed the triple point temperature (for deuterium, this is approximately 18.7 K): a fundamental limitation here is given by the thermal conductivity of the material itself. Additionally, the heat generated during extrusion due to viscosity must be removed by the cryocooler maintaining the cryogenic temperatures. At these temperatures, even a relatively slow extrusion that generates heating power on the order of a few watts is comparable to the cooling power available from a cryocooler.

[1] In its original form, Leachman's model is dimensionally inconsistent, as also noted by Fan et al. in [8]. In accordance with their choice for resolving this inconsistency, we also use a characteristic length of $d = 1$ mm here.

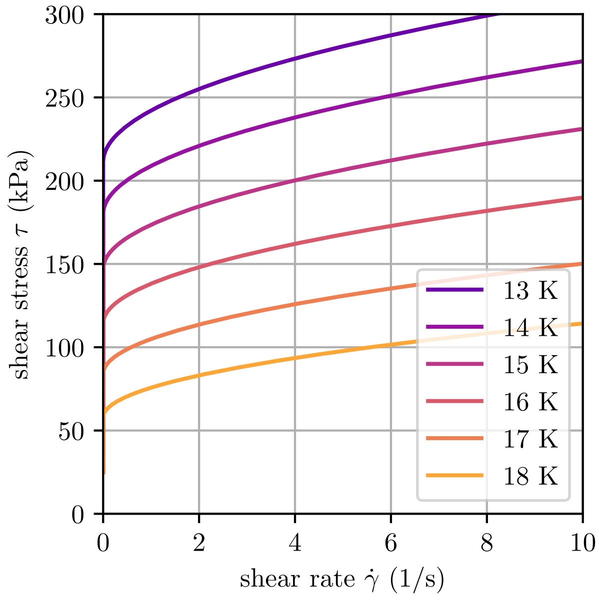

Figure 3: Temperature-dependence of the Herschel–Bulkley parameters in the Leachman model for solid deuterium, from 13 K to 18 K.

Therefore, predicting the thermal behaviour of solid deuterium during extrusion under various conditions is a crucial goal of a CFD model of solid deuterium under extrusion.

2.5 Investigated parameter space

The main goal of the present investigation is to evaluate the potential performance of different geometries for the converging region of the extruder. Currently, the reference device has a conical nozzle of length $h_2 = 24\,\text{mm}$, and for an extruder filled with the maximum amount of ice, piston velocities of around $0.1\,\text{mm/s}$ have been achieved so far. The question raised is whether alternative designs would fare better with higher volume flow rates, with respect to the maximum temperature and the viscous heating power, while the extrusion pressure remains at an acceptable level.

Besides the reference conical geometry with $h_2 = 24\,\text{mm}$, two different conical designs were evaluated, with $h_2 = 16\,\text{mm}$ and $32\,\text{mm}$, respectively. Additionally, based on observations at low extrusion rates, detailed below, two parabolic designs have also been evaluated, which were aimed at decreasing the maximum deuterium ice temperature inside the extruder. Fig. 4 shows the five different geometries overlaid.

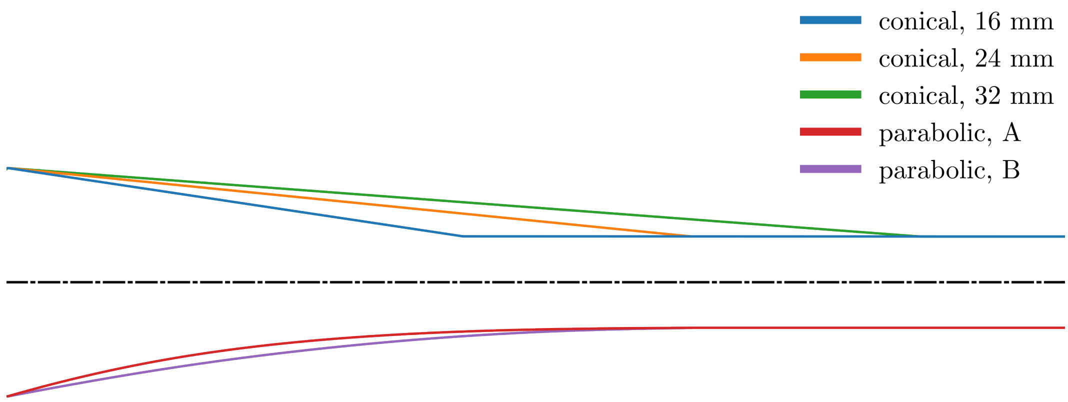

Figure 4: Contours of the different nozzle geometries overlaid.

3. Methods

3.1 Model, boundary conditions, mesh

For modelling the thermo-viscoplastic flow inside the extruder, a FEM-based CFD model is used, implemented in Ansys Polyflow. The flow domain is axisymmetric, therefore an axisymmetric 2D domain is modelled, as shown in Fig. 5 for the reference geometry. We neglect inertial effects, and assume a steady-state process. At the inlet, a uniform axial velocity and constant temperature is prescribed, corresponding to the movement of the piston inside the extruder. The outlet has an outflow-type boundary condition both mechanically and thermally.

Along the wall, a constant temperature of 15 K is imposed: this is realistic due to the very high thermal conductivity of copper at cryogenic temperatures and the active control of the extrusion device maintaining a set temperature of the extruder body, with 15 K being a typical extrusion temperature.

Based on our related experiments, for flow at the wall, a Navier-type slip condition is assumed, with a coefficient in the range $10^7\,\mathrm{Pa\,s\,m^{-1}} - 10^9\,\mathrm{Pa\,s\,m^{-1}}$ [15]. These related experiments also validated our model for the existing geometry, and for extrusion velocities and pressures up to about 0.5 mm/s and 7 MPa.

Clearly, laminar flow can be assumed, as the (apparent) Reynolds number of the flow is on the order of 10^{-10} or lower.

The mesh is a quadrilateral-dominant mesh – with an inflation layer capturing the velocity and temperature gradients outside the plug flow region – having a characteristic cell size of 0.12 mm and approx. 45 000 elements. A mesh independence study has been performed for the reference geometry.

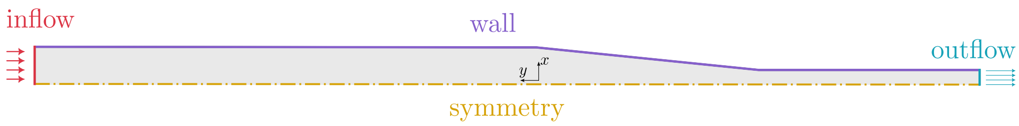

Figure 5: Illustration of the axisymmetric flow domain and the different boundary regions.

3.2 Numerical considerations

Since the temperature and flow fields are fully coupled in the simulation, achieving convergence is challenging due to the multiple strong nonlinearities present in the material models. To aid convergence, an evolution scheme is applied for both the viscosity and the thermal effects: i.e. the contributions of these effects are gradually increased from zero to their actual value by subsequent iterations.

Additionally, for numerical stability, the infinite effective viscosity resulting from the Herschel–Bulkley model is limited below a critical shear rate of $\dot{\gamma}_c = 0.1\,1/\mathrm{s}$ [16].

4. Results

The five geometries were evaluated for a range of flow rates, up to the point where the maximum temperature of the ice during extrusion exceeds the triple point temperature (detailed in Section 4.3). In these results, we have observed that there is a qualitative difference between the temperature distribution inside the nozzle for lower and for higher flow rates. Therefore, we first evaluate the results along this distinction.

To quantify the increased temperature inside the material, let us introduce the notation $\Delta T_{\max} := T_{\max} - T_{\mathrm{wall}}$ for the maximum temperature difference with respect to the prescribed boundary temperature.

4.1 Low flow rate

Fig. 6 illustrates the temperature distribution inside the three conical nozzle geometries. The prescribed inlet velocity in this case is 1 mm/s, corresponding to a volumetric flow rate of approx. 50 mm^3/s.

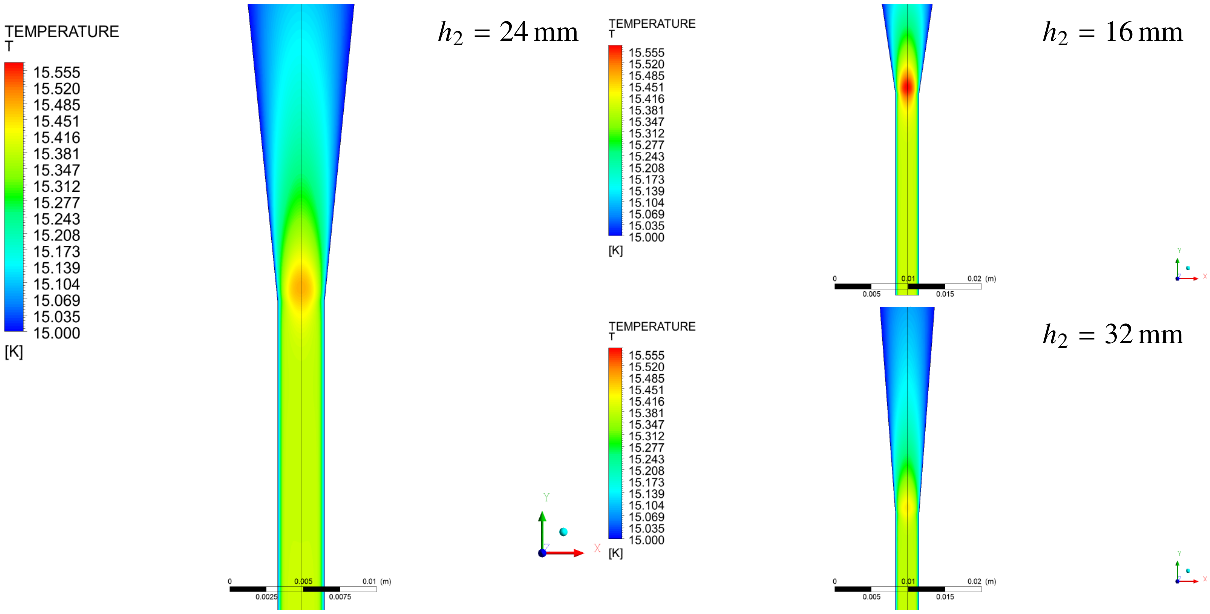

Figure 6: Temperature distribution inside the three conical nozzle geometries, for 1 mm/s inlet velocity.

In all three cases, a clear region of higher temperature develops at the bottom of the converging nozzle. The maximum temperature here decreases with increasing h_2, in accordance with the lower shear rates corresponding to a less sudden contraction.

Similar preliminary results inspired the development of a non-conical, parabolic nozzle geometry that, so to speak, smears the concentrated high shear rate and the resulting concentrated viscous heat generation along the flow by introducing a non-linear contraction of the diameter. Two versions were designed, denoted here as *parabolic A* and *parabolic B*, respectively: refer to Fig. 4 for a comparison.

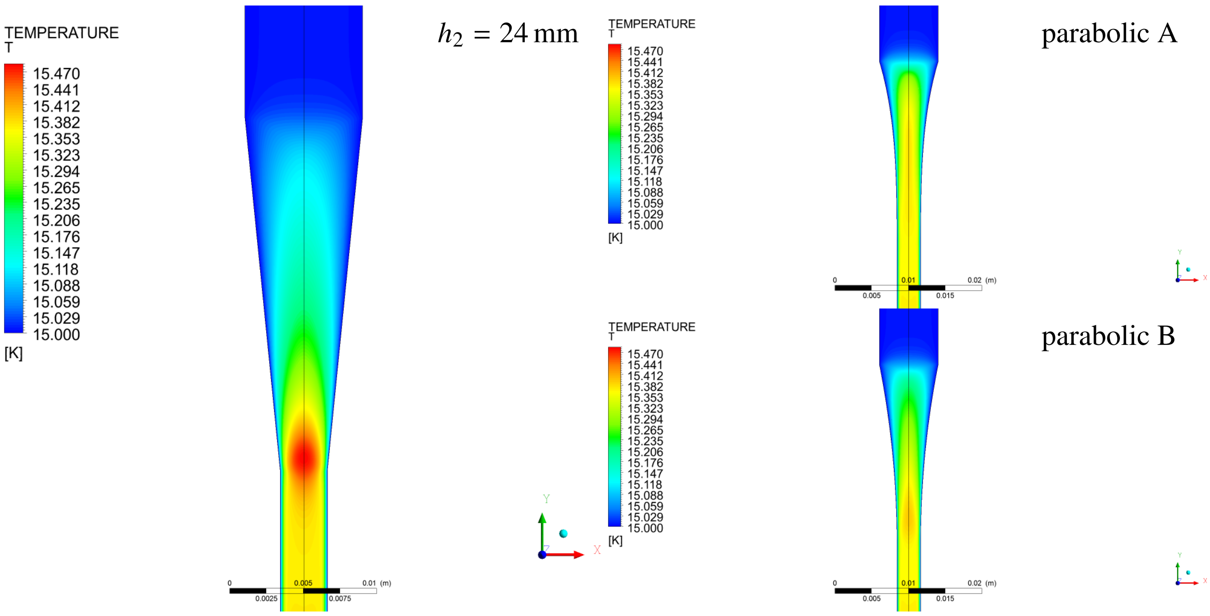

Figure 7: Temperature distribution inside the baseline (left) and the two parabolic (right) nozzle geometries, for 1 mm/s inlet velocity.

Fig. 7 illustrates the temperature distribution inside the two parabolic nozzles compared to the baseline $h_2 = 24$ mm conical nozzle. These designs indeed achieve a lower maximum temperature: compared to the baseline case, $\Delta T_{\max}$ decreases by 27% and 23% for the designs A and B, respectively. However, this comes at the cost of the viscous heating power increasing by 20% and 13%, respectively.

4.2 High flow rate

While it may be tempting to assume that the above phenomenon extends to higher flow rates, such an assumption would be incorrect. To illustrate this, let us first consider a higher flow rate case, with an inlet velocity of 2 mm/s corresponding to a volumetric flow rate of approx. $100\,\mathrm{mm}^3/\mathrm{s}$. Analogously to Fig. 6, we can observe the temperature distribution for the three conical geometries in Fig. 8. Clearly, the concentrated region of increased temperature in the converging region disappeared, and the region of highest temperature is now in the final, narrower part of the extruder.

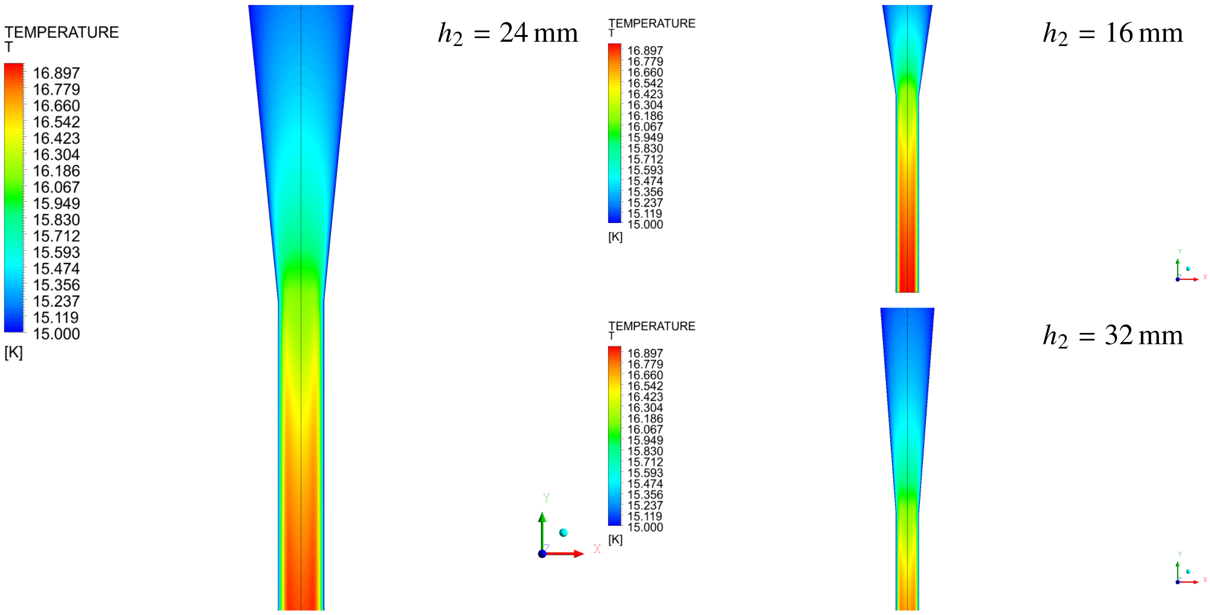

Figure 8: Temperature distribution inside the three conical nozzle geometries, for 2 mm/s inlet velocity.

This phenomenon seems to somewhat diminish the advantages of the parabolic designs: Fig. 9 illustrates this.

Fig. 10 qualitatively illustrates this phenomenon for the baseline geometry. As the flow rate increases, the region of higher temperature gradually extends and shifts further downstream, with the hot spot in the converging part eventually disappearing. This could be explained by the softening nature of the deuterium material model with increasing temperature: higher flow rates generate more heat, decreasing the effective viscosity, therefore decreasing the relative importance of the converging region, compared to the high shear rate that develops in the narrow tube.

4.3 Evaluation over various flow rates

To quantitatively evaluate the performance of the various geometries, we have performed a systematic parameter sweep over the applicable velocity ranges, with an identical wall and inlet temperature of 15 K. The flow rate has been increased for the subsequent simulations, until the maximum temperature inside the extruder reached the triple point temperature: at this point, the model is no longer valid, since no phase change is implemented.

Fig. 11 illustrates the development of the maximum temperature during extrusion for the five different geometries. It can be observed that for the low flow rates, the parabolic design is advantageous for decreasing the maximum temperature, but for higher flow rates, this advantage diminishes, and in fact

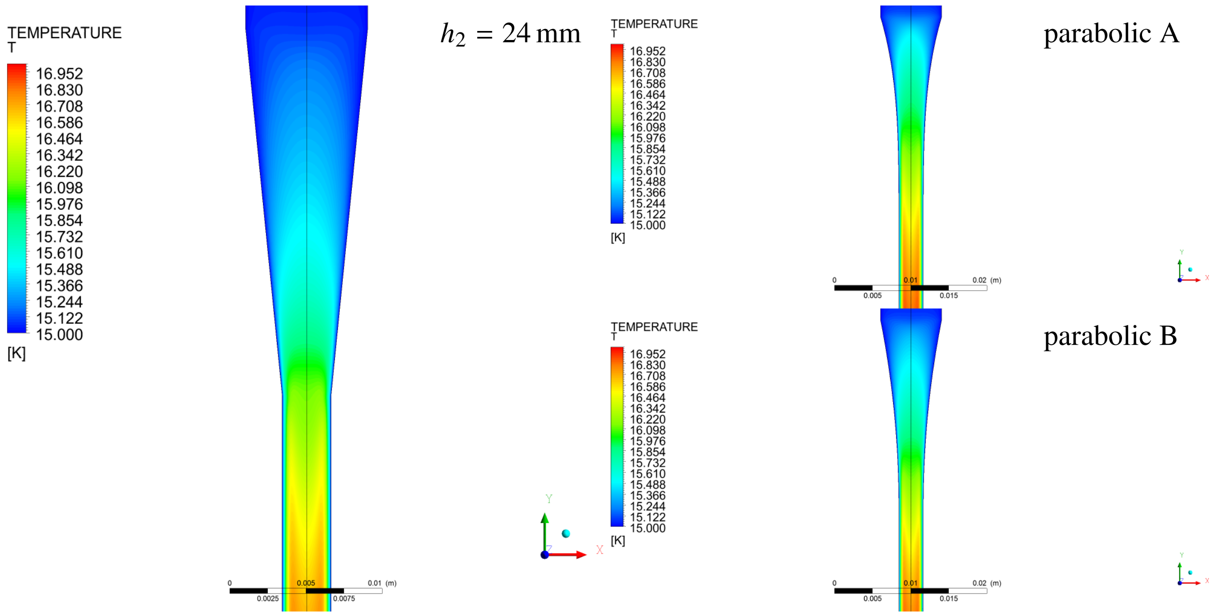

Figure 9: Temperature distribution inside the baseline (left) and the two parabolic (right) nozzle geometries, for 2 mm/s inlet velocity.

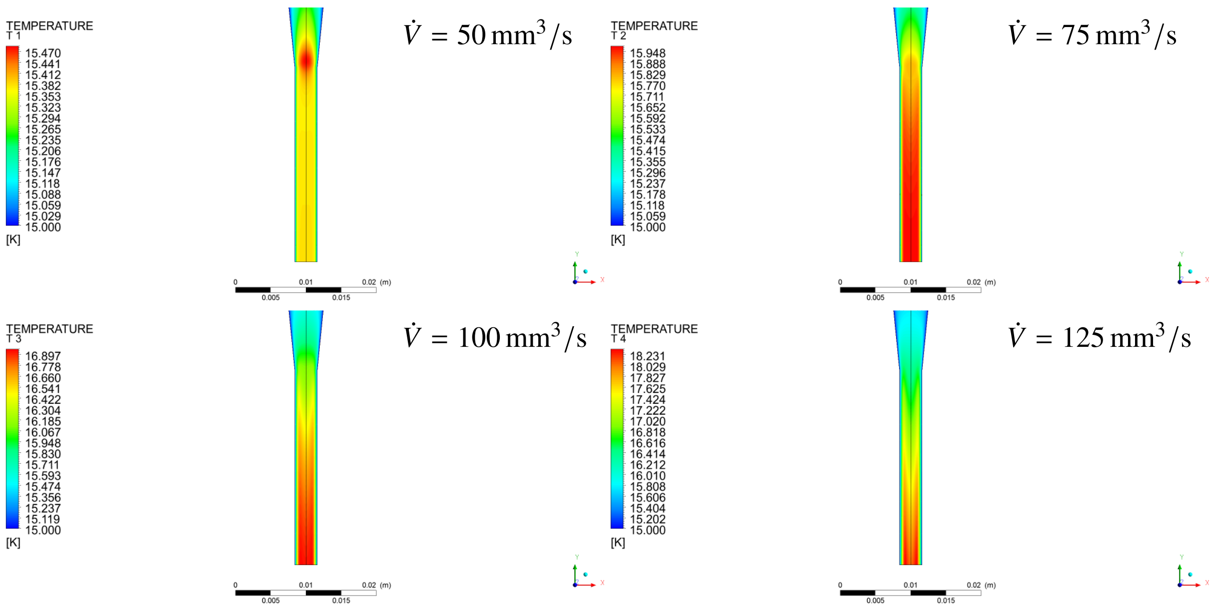

Figure 10: Temperature distribution inside the baseline conical nozzle, for various flow rates.

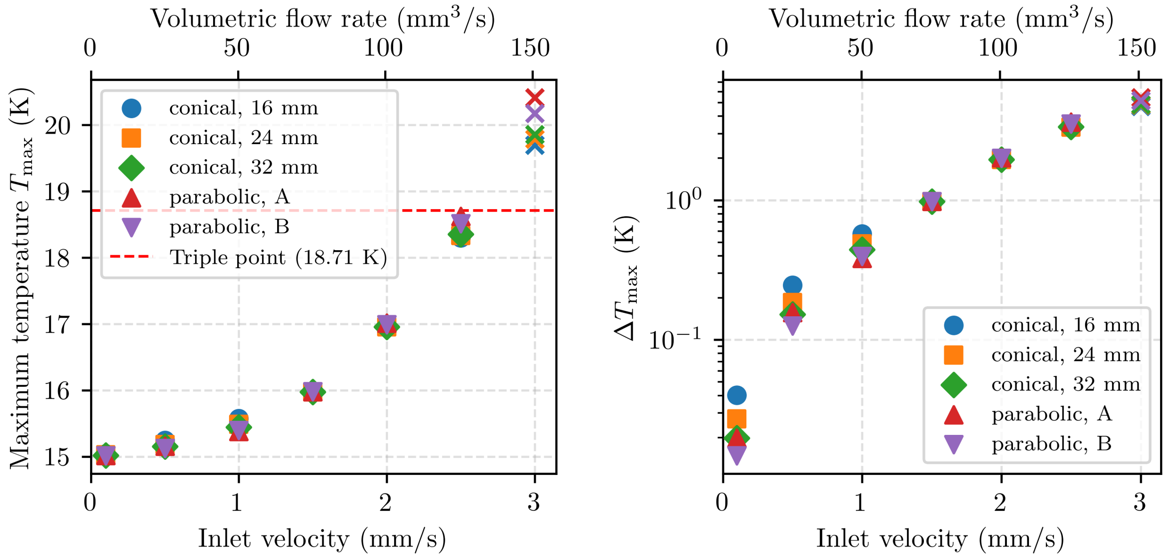

Figure 11: Maximum temperature inside the extruder for various flow rates and geometries. Left: $T_{\max}$. Right: $\Delta T_{\max}$ (logarithmic scale). Cases where the maximum temperature exceeded the triple point temperature are marked by $\times$.

reverses for the highest flow rates: for an inlet velocity of 2.5 mm/s, $T_{\max}$ is higher for the parabolic geometries than for the conical ones.

For the total heating power shown in Fig. 12, no reversal of the initial trend is observed: the viscous heating power for the parabolic geometries is consistently higher than for the conical geometries. The results suggest that a lower h_2 yields a lower viscous heating power, but a higher maximum temperature. Accordingly, the extrusion pressure, as also shown in Fig. 13, decreases for lower h_2 values.

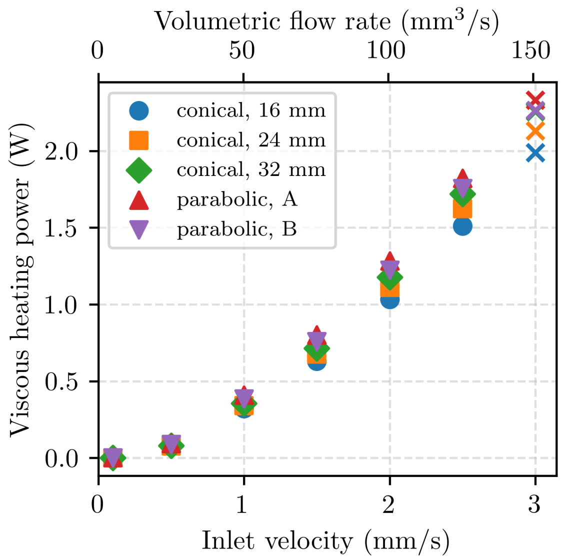

Figure 12: Viscous heating power for various flow rates and geometries. Cases where the maximum temperature exceeded the triple point temperature are marked by $\times$.

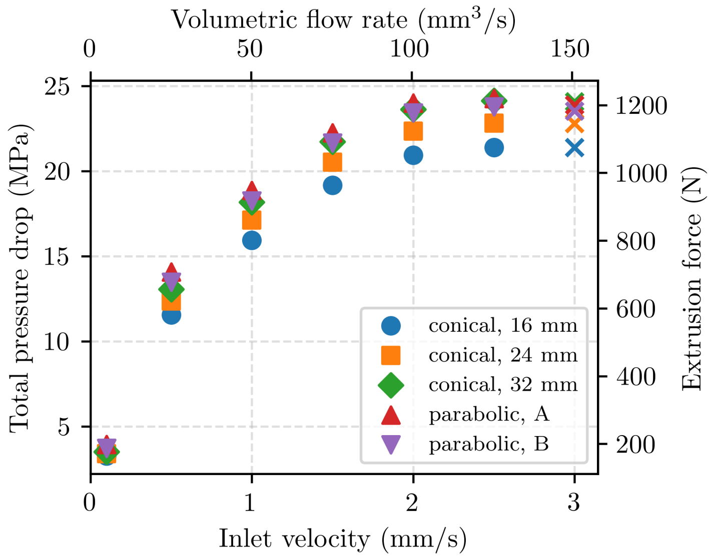

Figure 13: Extrusion pressure and equivalent force for various flow rates and geometries. Cases where the maximum temperature exceeded the triple point temperature are marked by ×.

5. Conclusion and Future Work

The performance of five different nozzle geometries has been evaluated for extruding solid deuterium at cryogenic temperatures. For this, a FEM-based CFD model has been developed that can resolve the nonlinear thermo-viscoplastic flow of deuterium ice.

The results indicate that a qualitatively different temperature field develops inside the extruder at low and at high flow rates. While, at lower flow rates, the high-temperature region is concentrated at the end of the contracting nozzle, at higher flow rates, the high-temperature region spreads and shifts further downstream, with the highest temperature observed in the narrow final tube of the extruder.

Based on the numerical results, it can be concluded that for lower flow rates, applying a parabolic nozzle geometry instead of a conical one decreases the maximum temperature, while resulting in higher extrusion pressures and higher viscous heating power. This advantage diminishes at higher flow rates, with the parabolic geometries creating a higher maximum temperature than conical nozzles at the highest flow rates.

Focusing on the conical nozzles, the presented simulations suggest that a shorter nozzle results in lower extrusion pressure and lower viscous heating power, but an increased maximum temperature inside the material. Therefore, when choosing the value of h_2 during design, a trade-off must be made based on the allowable maximum temperature and the available cooling power.

The current investigation has been limited to a wall temperature of 15 K. In future work, we plan to extend the evaluation to a range of other temperatures. Additionally, besides deuterium, the performance of different nozzles when used for the extrusion of protium should also be characterized. Based on the presented lessons, an optimized nozzle geometry that takes into account the different flow characteristics at increasing flow rates may also be developed, which would require a thorough evaluation across its entire operating range.

References

[1] E. Belonohy, O. J. W. F. Kardaun, T. Fehér, K. Gál, S. Kálvin, G. Kocsis, K. Lackner, P. T. Lang, and J. Neuhauser. A high field side pellet penetration depth scaling derived for ASDEX Upgrade. *Nuclear Fusion*, 48(6):065009, June 2008.

[2] Igor Vinyar, Jiansheng Hu, Soo-Hwan Park, Alexander Lukin, Xinjia Yao, Changzheng Li, Yue Chen, Pavel Reznichenko, and Hong-Tack Kim. Pellet injectors for EAST and KSTAR tokamaks. *Fusion Engineering and Design*, 124:779–782, November 2017.

[3] S. K. Combs and L. R. Baylor. Pellet-Injector Technology—Brief History and Key Developments in the Last 25 Years. *Fusion Science and Technology*, 73(4):493–518, May 2018.

[4] Jacob W. Leachman. *Thermophysical Properties and Modeling of a Hydrogenic Pellet Production System*. PhD thesis, The University of Wisconsin-Madison, 2010.

[5] Prashanth S Ravi Kumar and Senthil Kumar Arumugam. Non-Newtonian and non-isothermal numerical modelling of a twin screw hydrogen extruder with slip imposed boundary condition on the screw surface. *Fusion Engineering and Design*, 161:111896, December 2020.

[6] Vishal Gupta, Ranjana Gangradey, Samiran S. Mukherjee, Shashikant Verma, Avijit Dewasi, J. Mishra, Paresh Panchal, and Pratik A. Nayak. Validation of 3-D non-isothermal CFD simulation with experimental results for single-screw hydrogen extruder. *Cryogenics*, 124:103471, June 2022.

[7] H. T. Qiu, J. L. Hou, G. Z. Zuo, Y. Chen, Y. W. You, Q. C. Ren, J. Fu, and J. S. Hu. Design and heat transfer analysis of new single-screw pellet injector for EAST tokamak. *Fusion Engineering and Design*, 215:114962, June 2025.

[8] Yuqiao (Joy) Fan, Larry R. Baylor, and Steven J. Meitner. High-Fidelity CFD Modeling of Cryogenic Hydrogen Isotope Extrusion for Fusion Reactor Pellet Fueling. *Fusion Science and Technology*, 82(1-2):449–460, February 2026.

[9] Bence Longauer and Attila Piros. Development of a batch extruder for the testing of the EU-DEMO pellet puncher. *Fusion Engineering and Design*, 229:115833, August 2026.

[10] H. M. Roder, G. E. Childs, R. D. McCarty, and P. E. Angerhofer. *Survey of the Properties of the Hydrogen Isotopes Below Their Critical Temperatures*. Cryogenics Division Institute for Basic Standards National Bureau of Standards. Boulder , Colorado 80302, 1973.

[11] R. D. McCarty, J. Hord, and H. M. Roder. Selected Properties of Hydrogen, 1981.

[12] I. V. Vinyar and A. Ya. Lukin. Screw extruder for solid hydrogen. *Technical Physics*, 45(1):106–111, January 2000.

[13] Robert F. Mitchell, Stefan Miska, Bernt Sigve Aadnøy, and Society of Petroleum Engineers (U.S.), editors. *Fundamentals of Drilling Engineering*. Number v. 12 in SPE Textbook Series. Society of Petroleum Engineers, Richardson, TX, 2011.

[14] Rahman Ashena, Foued Badrouchi, Asad Elmgerbi, Siamak Mishani, Fatemeh Sotoudeh, and Sahand Nekoeian. Stepwise mathematical derivation of the Herschel–Bulkley laminar fluid flow equations—in pipes. *Journal of Petroleum Exploration and Production Technology*, 13(2):625–643, February 2023.

[15] D. M. Takács et al. Estimation of wall slip parameter during solid deuterium extrusion. *To be Published*, 2026.

[16] ANSYS, Inc. 9.2.2.8. Herschel–Bulkley Law. In *Ansys Polyflow Classic User's Guide*. ANSYS, Inc., Canonsburg, PA, 2025.